Control of vortex-induced vibration using a pair of synthetic jets: Influence of active lock-on

Cite as: Phys. Fluids **29**, 083602 (2017); https://doi.org/10.1063/1.4996231
Submitted: 01 February 2017 . Accepted: 12 July 2017 . Published Online: 01 August 2017

Chenglei Wang, Hui Tang, Simon C. M. Yu, and Fei Duan

Control of vortex-induced vibration using a pair of synthetic jets: Influence of active lock-on

Chenglei Wang,[1,2] Hui Tang,[2,a)] Simon C. M. Yu,[3] and Fei Duan[1]
[1]*School of Mechanical and Aerospace Engineering, Nanyang Technological University, Singapore 639798, Republic of Singapore*
[2]*Department of Mechanical Engineering, The Hong Kong Polytechnic University, Kowloon, Hong Kong, China*
[3]*Singapore Institute of Technology, Singapore 179104, Republic of Singapore*

(Received 1 February 2017; accepted 12 July 2017; published online 1 August 2017)

While conventional vortex-induced vibration (VIV) of bluff bodies is suppressed through reducing the strength of asymmetric vortex shedding, it can also be mitigated by shifting the vortex shedding frequency away from the natural frequency of the body structures using active lock-on. Recently Du and Sun ["Suppression of vortex-induced vibration using the rotary oscillation of a cylinder," Phys. Fluids **27**, 023603 (2015)] utilized periodical rotation to induce the lock-on of the frequency of vortex shedding from a transversely vibrating cylinder to the rotation frequency and demonstrated successful VIV suppression. However, questions were raised from this investigation: Does the occurrence of active lock-on always suppress VIV? If not, how to ensure the appropriate usage of active lock-on for VIV suppression? To address these research questions, a numerical investigation is conducted on the active VIV control of a circular cylinder using a pair of synthetic jets (SJs) at a low Reynolds number of 100. The SJ pair operates with various phase differences over a wide frequency range so that the influence of various lock-on can be investigated. It is found that the VIV control can be affected not only by the occurrence of the primary lock-on but also by the occurrence of other lock-on such as secondary and tertiary lock-on. The occurrence of lock-on does not always result in successful VIV suppression. Sometimes it even causes the augmentation of VIV. Compared to the VIV suppression using the conventional vortex-strength-reduction method, the control by the means of active lock-on seems less effective. *Published by AIP Publishing.* [http://dx.doi.org/10.1063/1.4996231]

I. INTRODUCTION

Flow past a bluff body can cause asymmetric vortex shedding when the Reynolds number exceeds a critical value, resulting in dynamic loading on the body. When the vortex shedding frequency matches the body structure's natural frequency, large-amplitude vibrations may occur, a well-known phenomenon called vortex-induced vibration (VIV). In this case, catastrophic failures to the structure may happen. Since VIV occurs in many engineering applications, such as bridges, transmission lines, heat exchangers, and offshore structures, it needs to be attenuated through effective control in order to protect the relevant structures.

Numerous VIV control methods were proposed in the literature, which can generally be classified into two major categories: passive (no power input is required) and active (power input is required) controls.[1] Realized through geometry modification, passive VIV control is easy to implement and hence has been extensively applied.[1–4] However, the passive VIV control is usually effective in narrow operational ranges and cannot provide on-demand control. By contrast, the active VIV control can perform more adaptively and effectively by introducing a small and tunable amount of energy into the ambient flow. Many active control methods have been utilized to suppress VIV through manipulating the asymmetric wakes behind bluff bodies.[5–11] Most of them work by directly reducing the strength of asymmetric vortices and resulting exciting forces, e.g., the moving surface boundary-layer control (MSBC),[5] windward-suction-leeward-blowing (WSLB),[6,7] synthetic jets (SJ),[8] pure suction,[9] and pure blowing.[10]

Other than using the vortex-strength-reduction methods, VIV can also be mitigated by shifting the vortex shedding frequency away from the natural frequency of the body structures.[11] An effective way for the frequency shift is to provoke lock-on—nonlinear phenomena—by introducing periodic external forcing. For flows past a circular cylinder, a typical bluff body, three major types of lock-on have been widely reported, i.e., the primary, secondary, and tertiary lock-on,[12–14] where the vortex shedding frequency is attracted to the forcing frequency, its 1/2 or its 1/3, respectively. Furthermore, for a cylinder immersed in a cross flow, it was found that the type of lock-on mainly depends on the phase difference between the forcing pair exerted over the cylinder's two half surfaces that are divided by the cylinder's streamwise centerline.[14,15] Here the forcing pair is defined as in-phase when they are symmetric about the cylinder's streamwise centerline and anti-phase when they are anti-symmetric. It was reported that the primary and tertiary lock-on can be induced when the forcing phase difference is π (i.e., anti-phase), such as when the cylinder undergoes rotational or transverse oscillations[13] or

a)h.tang@polyu.edu.hk

anti-phase excitation of a SJ pair,[15] and the secondary lock-on can be provoked when the forcing phase difference is 0 (i.e., in phase), such as when the cylinder undergoes streamwise oscillations[14] or in-phase excitation of a SJ pair.[15]

Recently, Du and Sun[11] applied periodical rotation (i.e., anti-phase external forcing) to a transversely vibrating cylinder at frequencies in the vicinity of its natural frequency and successfully demonstrated the attraction of the vortex shedding frequency to the forcing frequency as well as the resulting VIV suppression. Although having also mentioned that at certain forcing frequencies, the lock-on may result in augmentation instead of suppression of VIV, they did not further elaborate on this. This leads to immediate questions: Does the occurrence of active lock-on always suppress VIV? If not, how to ensure the appropriate usage of active lock-on for VIV suppression? To address these questions, in the present study, we utilize a SJ pair over a relatively large range of forcing frequencies to induce active lock-on and influence the transverse VIV of a circular cylinder. In addition to its strength, the SJ pair is also tuned to operate with various phase differences so that the influence of primary, secondary, and tertiary lock-on can be studied with the same setup.

This paper is organized as follows: The problem setup and numerical method are described in Sec. II, the influence of various lock-on on VIV is presented and discussed in Sec. III, in which more flow physics in the wakes for several represented cases is revealed using the dynamic mode decomposition (DMD) analysis, and a conclusion is given in Sec. IV.

II. PROBLEM DESCRIPTION AND METHODOLOGY

A. Problem description

In this study, the VIV of a circular cylinder is controlled at a low cylinder-diameter-based Reynolds number, i.e., $Re = 100$. Under this condition, a two-dimensional Kármán vortex street forms behind the cylinder.[16] The cylinder is immersed in a uniform flow, connecting to a spring along the cross-flow direction but being refrained in the streamwise direction, as depicted in Fig. 1. Accordingly, the cylinder can only move in the cross-flow direction, and its dynamics is governed by

$$m\ddot{y}_o + Ky_o = F_L, \tag{1}$$

where y_o is the cylinder's y displacement, m is the mass of the cylinder, K is the stiffness of the spring, and F_L is the lift force experienced by the cylinder. To separate the added-mass effect from the lift force, F_L is further decomposed into two force components[17]

$$F_L = F_A + F_V, \tag{2}$$

where F_A is the potential added-mass force and F_V is the remaining force stemming from the formation and shedding of vortices. The former is the reaction force exerted by the passively accelerated fluid around the cylinder and can be evaluated by

$$F_A = -C_A m_d \ddot{y}_o, \tag{3}$$

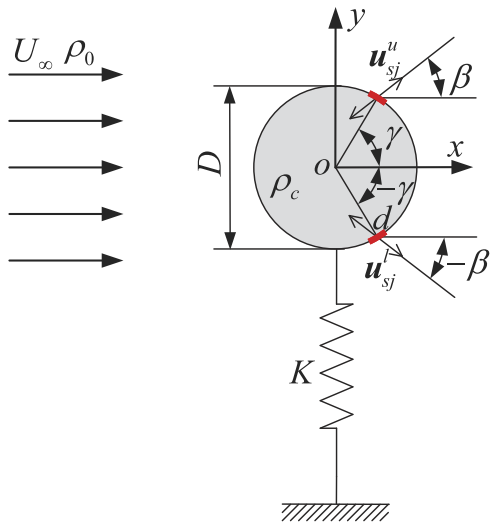

FIG. 1. Schematic of a transversely oscillating cylinder equipped with a SJ pair. U_∞ is the freestream velocity, ρ_0 is the fluid density, D is the diameter of the cylinder, ρ_c is the density of the cylinder, and K is the stiffness of the spring. The two red line sections represent the SJ pair, β represents the SJ orientation, γ represents the SJ azimuthal angle, d represents the SJ width, and $\boldsymbol{u}^u_{sj}$ and $\boldsymbol{u}^l_{sj}$ represent the velocities of the upper and lower SJs relative to the oscillating cylinder, respectively.

where C_A is the potential flow added-mass coefficient, and m_d is the displaced fluid mass,

$$m_d = \frac{\pi \rho_0 D^2}{4}, \tag{4}$$

where ρ_0 is the fluid density and D is the cylinder diameter. Therefore, Eq. (1) can be rewritten as

$$(m + C_A m_d)\,\ddot{y}_o + Ky_o = F_V. \tag{5}$$

Normalizing Eq. (5) gives rise to

$$\frac{\mathrm{d}^2 y_o^*}{\mathrm{d}t_r^{*2}} + \left(\frac{4\pi^2}{U_R^2}\right) y_o^* = \frac{2C_V}{\pi\,(m^* + C_A)}, \tag{6}$$

where $y_o^* = y_o/D$, $t_r^* = U_\infty t/D$, and U_∞ is the freestream velocity. U_R is the reduced velocity defined as

$$U_R = \frac{U_\infty}{f_N D}, \tag{7}$$

where f_N is the natural frequency of the present mass-spring system in fluid,

$$f_N = \frac{1}{2\pi}\sqrt{\frac{K}{m + C_A m_d}}. \tag{8}$$

m^* is the cylinder-fluid mass ratio defined as

$$m^* = \frac{m}{m_d}. \tag{9}$$

In Eq. (6), C_V is the vortex force coefficient defined as

$$C_V = \frac{2F_V}{\rho_0 U_\infty^2 D}. \tag{10}$$

Assuming that C_V varies harmonically

$$C_V\,(t_r^*) = A_{C_V} \cos\left(\frac{2\pi f^* t_r^*}{U_R}\right), \tag{11}$$

one can get the analytical solution of Eq. (6),[18]

$$y_o^*(t_r^*) = \frac{A_{C_V} U_R^2}{2\pi^3 (m^* + C_A)(1 - f^{*2})} \cos\left(\frac{2\pi f^* t_r^*}{U_R}\right) + C_1 \cos\left(\frac{2\pi t_r^*}{U_R}\right) + C_2 \sin\left(\frac{2\pi t_r^*}{U_R}\right), \quad (12)$$

where A_{C_V} is the amplitude of C_V fluctuations and $f^* = f/f_N$ is the normalized frequency. C_1 and C_2 are the constants determined by the cylinder's initial conditions. The first term of this solution is related to the vortex forcing through A_{C_V}, whereas the second and third terms are undamped natural vibrations due to non-equilibrium initial conditions. According to the first term, the VIV amplitude increases with vortex force amplitude A_{C_V} or when f^* approaches 1. Furthermore, the forced vibration is in-phase with the vortex force if $f^* < 1$ and anti-phase if $f^* > 1$. Note that although in general C_V variation is not a single-frequency harmonic as assumed in Eq. (11), the relations revealed from Eq. (12) are still valid because any given C_V variation can be decoupled into multiple harmonics and hence can be used to explain the VIV control effectiveness under various forcing conditions.

The control of the cylinder's cross-flow VIV is realized through the operation of a pair of SJs. The SJ pair is implemented on the leeward side of the cylinder, symmetrical about the cylinder's horizontal centerline with an azimuthal angle (γ), as depicted in Fig. 1 (represented by two red line sections). Assuming that the SJ pair operates with the same excitation frequency (f_{sj}) and velocity amplitude (U_{sj}), the time-dependent velocities of the upper and lower SJs relative to the oscillating cylinder are given as

$$\boldsymbol{u}_{sj}^u = U_{sj} \sin(2\pi f_{sj} t + \phi_u)(\cos\beta, \sin\beta), \quad (13)$$

$$\boldsymbol{u}_{sj}^l = U_{sj} \sin(2\pi f_{sj} t + \phi_l)(\cos\beta, -\sin\beta), \quad (14)$$

where β is the jet orientation angle relative to the cylinder's horizontal centerline. ϕ_u and ϕ_l are the operating phase angles of the upper and lower SJs, respectively, from which a phase difference between these two SJs can be defined as

$$\Delta\phi = \phi_l - \phi_u, \quad (15)$$

where ϕ_u is set as 0 throughout this study, unless otherwise stated. Normalizing f_{sj} using f_N gives a non-dimensional SJ excitation frequency

$$f_{sj}^* = \frac{f_{sj}}{f_N}. \quad (16)$$

The SJ strength is quantified by a momentum coefficient defined as

$$C_\mu = \frac{2U_{sj}^2 d}{U_\infty^2 D}, \quad (17)$$

where d is the width of SJ slots. In this study, it is set as 1/72 of the cylinder perimeter, i.e., $d = \pi D/72$.

In this study, the cylinder-fluid mass ratio (m^*) and reduced velocity (U_R) are fixed at 2.55 and 5.9, respectively, to ensure the cylinder's relatively large vibrations that, however, are difficult to suppress.[11] Note that the potential flow added-mass coefficient (C_A) is affected by the cylinder's motion, such as its vibration amplitude and frequency,[19] as well as by the operation of the SJ pair. Consequently, in this study, the actual natural frequency of the mass-spring system in fluid varies slightly in different cases. To ensure consistent comparison and convenience of discussion, however, the nominal natural frequency (f_N) is calculated using $C_A = 1.0$ for all cases, which is usually adopted for circular cylinders as suggested by Govardhan and Williamson.[17]

B. Methodology

To facilitate this study, the incompressible D2Q9 MRT LBE model,[20] i.e., the two-dimensional incompressible multiple-relaxation-time (MRT) lattice Boltzmann equation model with nine discrete velocities, is employed to simulate the two-dimensional flow around the circular cylinder. The MRT multi-block scheme[21] is applied to enhance the computational efficiency while maintaining sound accuracy. Furthermore, the interpolated half-way bounce back scheme[22] is incorporated to deal with curved boundaries, and the corrected momentum exchange method[23] is employed for an accurate prediction of the aerodynamic forces on the cylinder.

Throughout this study, the computational domain is set as $60D(\mathrm{L}) \times 20D(\mathrm{W})$ with a uniform flow flowing from the left to the right at a speed U_∞ as shown in Fig. 2. The circular cylinder is initially placed on the channel centerline and $20D$ away from the inlet boundary. Additionally, the entire computational domain is divided into four sets of blocks with the mesh density being increased by a factor of 2 as the block number increases. Around the cylinder, the finest block (block 4) with mesh spacing $\Delta x = D/60$ is used. The velocity of the uniform incoming flow is set as $U_\infty/c = 0.01$, corresponding to the non-dimensional time step $U_\infty \Delta t/D = 1/6000$, where c is the lattice velocity and Δt is the unit time step.

The boundary conditions are also shown in Fig. 2. At the inlet boundary, the non-reflecting inlet boundary condition[24] is used, whereas at the outlet boundary, the homogenous Neumann boundary condition is implemented. On the top and bottom walls, the Dirichlet boundary condition is applied with the x-component velocity U_∞ and the y-component velocity 0. The SJ actuators are represented by a number of nodes on the cylinder surface, and the time-dependent SJ velocities are realized by enforcing $\boldsymbol{u}_{sj}^u$ and $\boldsymbol{u}_{sj}^l$ on these nodes. The details of the algorithm and its validation can be found in our previous work.[7,8]

C. Case summary

According to Eqs. (13)–(17), the capability of the SJ pair in controlling the cylinder's cross-flow VIV depends on five

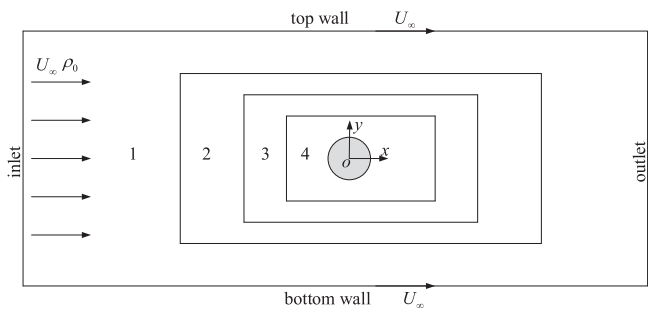

FIG. 2. Computational domain with multi-block arrangement (not in scale).

TABLE I. Summary of selected SJ based VIV control cases.

Parameter	Values
C_μ	0.537, 0.955, 2.149
f_{sj}^*	0.4, 0.6, 0.8, 1, 1.1, 1.2, 1.3, 1.4, 1.6, 1.7, 1.8, 1.9, 2, 2.1, 2.2, 2.3, 2.4, 2.6, 2.7, 2.8, 2.9, 3, 3.1, 3.2, 3.3, 3.4, 4, 5, 6, 7
$\Delta\phi$	0, $\pi/4$, $\pi/2$, $3\pi/4$, π

key parameters, i.e., the location (γ), orientation (β), momentum coefficient (C_μ), excitation frequency (f_{sj}^*), and phase difference ($\Delta\phi$) of the SJ pair. In this study, the first two parameters are fixed as follows: $\gamma = 50°$, at which the SJs can effectively interact with the shear layer so as to suppress the cross-flow VIV;[8] $\beta = 0°$, i.e., the SJs are issued horizontally. In order to induce the primary, secondary, and tertiary lock-on, f_{sj}^* varies from 0.4 to 7, covering 30 different values, and $\Delta\phi$ is set from 0 to π with an interval of $\pi/4$. Furthermore, 3 C_μ values are selected, i.e., $C_\mu = 0.537$, 0.955, and 2.149 so that the effect of momentum coefficient can also be studied. Therefore, in total, 271 cases are simulated in the present study, including one unforced case. All the SJ controlled cases are summarized in Table I.

III. RESULTS AND DISCUSSIONS

A. Unforced case

Serving as a benchmark, the simulation results from the unforced case are presented in this section. Figure 3 shows an instantaneous wake pattern behind the vibrating cylinder, in which the contour of the normalized vorticity (defined as $\omega^* = \omega D/U_\infty$, where ω is the vorticity) is superimposed by the vortex lines identified using the λ_{ci} criterion.[25] In this case, vortices grow alternatively from the upper and lower sides of the cylinder, interact with each other, and shed periodically to form a 2S-mode wake.[26] Consequently, the lift and drag forces experienced by the cylinder vary periodically with time, and the phase diagram of the lift against drag coefficients (respectively, defined as $C_L = \frac{2F_L}{\rho_0 U_\infty^2 D}$ and $C_D = \frac{2F_D}{\rho_0 U_\infty^2 D}$) forms a figure "8."

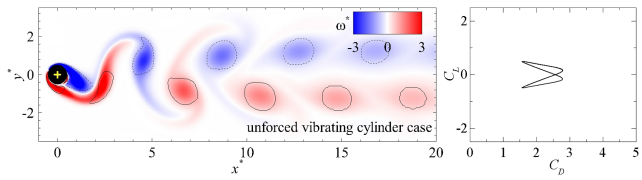

FIG. 3. Wake pattern and C_L-C_D phase diagram for the unforced case. The solid and dashed loop lines are $\lambda_{ci} = 0.2$ isolines representing vortices enclosing positive and negative vorticities, respectively.

The periodically varying lift force drives the cylinder to oscillate transversely with an amplitude of $A_y^* = 0.545$ and a frequency of $f^* = 1.1$, as revealed in Figs. 4(a) and 4(c). As a key component of the lift force, the vortex force also varies with the same period but has two major frequency components, i.e., $f^* = 1.1$ and 3.3, as revealed in Figs. 4(b) and 4(d). This indicates the nonlinearity of the vortex force. Comparing Figs. 4(a) and 4(b) also reveals that the vortex force is anti-phase with the cylinder's displacement, meaning that it performs as a restoring force in this dynamic system. This observation is consistent with what has been revealed in Eq. (12), in which the coefficient of the first term on the right-hand side becomes negative when $f^* > 1$.

Note that the wake pattern shown in Fig. 3 is taken at the instant when the cylinder approaches its equilibrium position from the lower side after the system achieves its periodic steady state. This instant almost coincides with the instant when the lift decreases to zero. Hereafter in this study, all the wake patterns are also presented at this instant. Furthermore, the operation of the SJs in all the controlled cases starts at this instant (defined as $t^* = t/T_N = 0$, where T_N is the nominal natural period of the mass-spring system in static fluid). Although not presented here for the sake of brevity, an investigation has been conducted to confirm that the SJ initial conditions, including the actuation timing and the starting phase angle, do not affect the cylinder's steady-state vibration amplitude.

B. VIV controlled by the anti-phase SJ pair

When the anti-phase (i.e., $\Delta\phi = \pi$) SJ pair is applied, the cylinder's transverse VIV amplitude (A_y^*) varies with the SJ frequency (f_{sj}^*) and strength (C_μ), as presented in Fig. 5. From the three f_{sj}^*-A_y^* curves that correspond to three C_μ values, it is seen that the operation of SJs generally reduces the VIV amplitude, and the control becomes more effective with the increase of C_μ. In addition, these three curves all follow a similar trend: peaks appear near two specific frequencies, i.e., $f_{sj}^* = 1$ and 3, where the VIV amplitude becomes larger than 0.545 as in the unforced case (represented by the dashed horizontal line) and the curves gradually level off when the SJs operate at frequencies greater than 4. Because of this similarity, in the following the discussions will only be focused on the curve with the

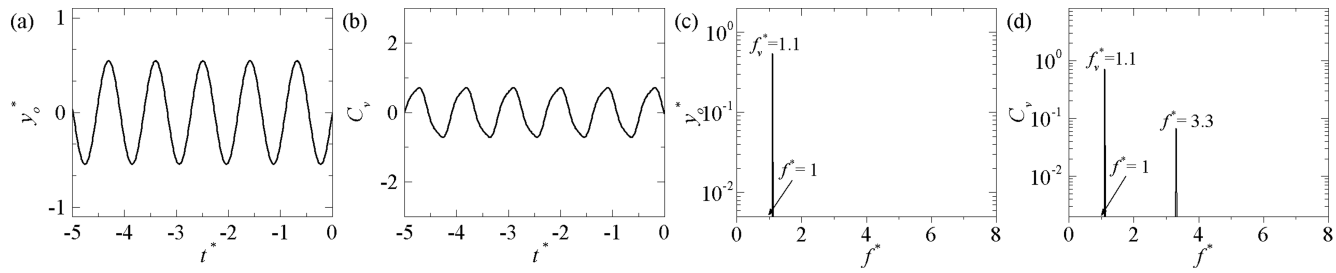

FIG. 4. Time histories [(a) and (b)] and frequency spectra [(c) and (d)] of the cylinder's normalized y displacement (y_o^*) and of the vortex force coefficient (C_V) for the unforced case. The spectral analysis is performed over 35 VIV periods after the flow reaches its steady state.

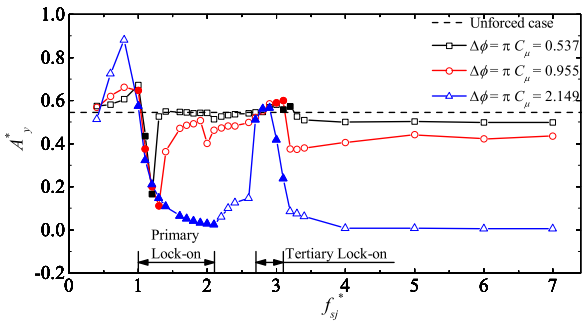

FIG. 5. Variations of the cylinder's transverse VIV amplitude (A_y^*) against the SJ frequency (f_{sj}^*) when the anti-phase SJ pair is applied for the control. Open symbols represent the non-lock-on cases and solid symbols represent the lock-on cases.

largest SJ strength (i.e., $C_\mu = 2.149$, in blue). In addition, to help explain the cause of variations, the time histories and spectra of the cylinder's transverse displacement (y_o^*) and of the vortex force coefficient (C_V) for several key cases along this curve are also presented in Fig. 6. Note that the time histories shown in the first two columns of Fig. 6 span from $t^* = -2$ to 22, covering the entire three stages of the dynamics, i.e., the variations before the SJ control, the transient process right after the control, and the steady-state variations after the control. However, the spectra shown in the last two columns of Fig. 6 are not obtained from the same time span. Instead, they are obtained by analyzing the data from the third stage, i.e., after the controlled system achieves its steady state. More specifically, data from 35 VIV periods for lock-on and high-frequency cases and data from 100 nominal natural periods for non-lock-on cases are used.

Figure 5 reveals that, when the SJ frequency is less than unity (i.e., $f_{sj}^* < 1$), the cylinder's vibration amplitude increases with the SJ frequency, and most of the investigated cases in this frequency range have an amplitude greater than that in the unforced case. This variation trend can be explained from two aspects. First, the operation of the SJ pair in this frequency range does not induce any lock-on, and hence a non-zero vortex force exists at the cylinder's natural frequency (i.e., $f^* = 1$). This is evidenced by the time histories and spectra of the cylinder's transverse displacement and vortex forces in a selected case at $f_{sj}^* = 0.6$, as shown in Figs. 6(a1)–6(d1). In addition, although not presented, simulation results of all cases in this range show that this $f^* = 1$ component of vortex force increases with forcing frequency. This explains the increase of VIV amplitude. Second, the operation of the SJ pair also induces non-zero vortex force at the SJ frequency. According to Eq. (12), this $f^* < 1$ component of vortex force is always in-phase with the cylinder's displacement, indicating that it serves as a driving force and injects energy into the system. As such, the resulting VIV amplitude is generally larger than that in the unforced case.

When the SJ pair operates between $f_{sj}^* = 1$ and 2.1, the primary lock-on occurs, where the vortex shedding frequency is attracted to the SJ frequency. In the curve shown in Fig. 5, the corresponding simulation cases are marked using solid symbols. It is seen that, as the SJ frequency moves away from the cylinder's nominal natural frequency $f^* = 1$, the transverse VIV amplitude reduces dramatically, reaching a value very close to zero. The reason for this reduction is obvious: the occurrence of lock-on shifts the frequency of vortex shedding and hence of the vortex force away from the cylinder's nominal natural frequency. This is evidenced from the vortex force spectra in the $f_{sj}^* = 1$, 1.2, and 2 cases shown in Figs. 6(d2)–6(d4). It is also seen that, when the SJ pair operates at the cylinder's nominal natural frequency 1, the VIV amplitude ($A_y^* = 0.575$) is higher than 0.545 in the unforced case, even though the vortex force in the former case is significantly smaller. This can be well explained by the first term of Eq. (12), which indicates that both the amplitude and frequency of vortex force affect the VIV amplitude. In this case, since the vortex forcing frequency appearing in the denominator is attracted to 1 from 1.1 due to the SJ induced lock-on, the resulting VIV amplitude becomes more severe even with a much smaller vortex forcing amplitude. The results in this frequency range clearly demonstrate that the occurrence of the primary lock-on can successfully suppress the transverse VIV if the SJ frequency moves away from the cylinder's nominal natural frequency.

The primary lock-on does not occur any more as the SJ pair operates at frequencies higher than 2.1. As a result, the $f^* = 1$ component of vortex force revives, as demonstrated in Fig. 6(d5) for the $f_{sj}^* = 2.6$ case. This directly results in the reoccurrence of transverse VIV, as confirmed in Fig. 6(a5). However, due to the interruption of higher-frequency SJs, the shear layers developed on the cylinder evolve only into smaller and weaker vortices, as shown in Fig. 7(b). Hence the VIV amplitude becomes much smaller than that in the unforced case. As the SJ frequency further increases, the interruption of vortex formation becomes more severe and so does the reduction of the VIV amplitude. This trend is confirmed by the level off of the VIV amplitude to a value very close to zero when the SJ frequency approaches 4, as revealed in Fig. 5. From the $f_{sj}^* = 5$ case shown in Figs. 6(a7)–6(d7) as well as Fig. 7(c), it is also seen that at such a high operation frequency, the SJ pair turns to dominate the flow, completely eliminating the vortex force component at $f^* = 1$.

Interestingly, however, in the frequency range of $f_{sj}^* > 2.1$, the VIV amplitude does not decrease monotonically as expected. Instead, another peak appears near $f_{sj}^* = 3$, which is associated with a new lock-on phenomenon, i.e., the tertiary lock-on. It is found that, when the SJ pair operates between $f_{sj}^* = 2.7$ and 3.1, the tertiary lock-on occurs (also represented by solid symbols in Fig. 5), where the vortex shedding frequency is attracted to 1/3 of the SJ frequency.[15] This attraction is evidenced in a representative case shown in Figs. 6(a6)–6(d6), where the frequency of vortex shedding shifts from $f^* = 1$ to 0.93, i.e., 1/3 of the SJ frequency 2.8. However, since in this range the 1/3 SJ frequency is so close to the cylinder's nominal natural frequency (i.e., $f^* = 1$) that the transverse VIV still occurs, the second peak appears in Fig. 5. This result indicates that the occurrence of lock-on may not always lead to the suppression of VIV, and sometimes it even augments the VIV.

From the above results, one can see that, to suppress the cylinder's transverse VIV, the anti-phase SJ pair should be operated with sufficient strength either in the primary

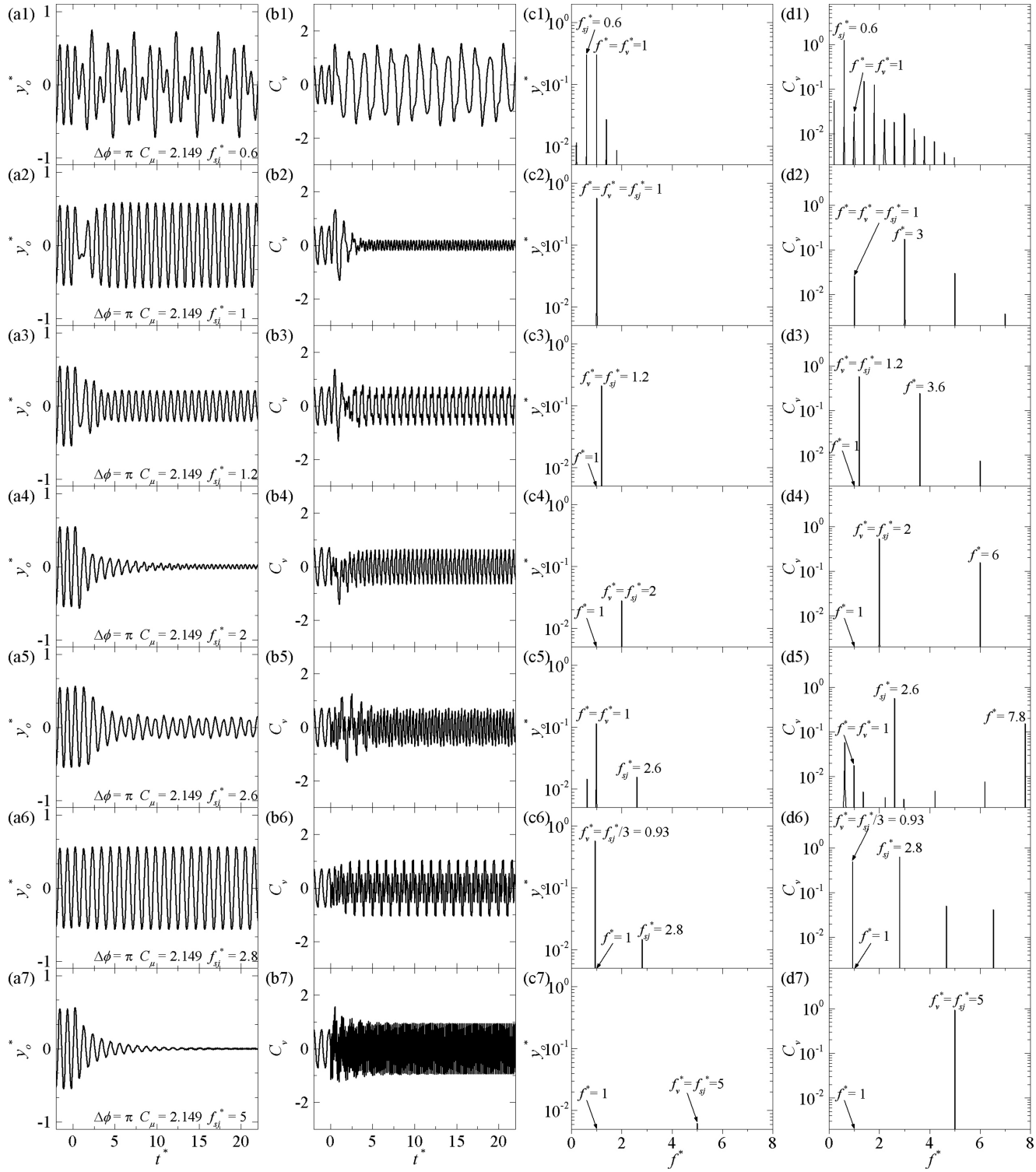

FIG. 6. Time histories and frequency spectra of the normalized cylinder's y-displacement (y_o^*) and the cross-flow vortex force coefficient (C_V) for $f_{sj}^* = 0.6$ [(a1)–(d1)], $f_{sj}^* = 1$ [(a2)–(d2)], $f_{sj}^* = 1.2$ [(a3)–(d3)], $f_{sj}^* = 2$ [(a4)–(d4)], $f_{sj}^* = 2.6$ [(a5)–(d5)], $f_{sj}^* = 2.8$ [(a6)–(d6)], and $f_{sj}^* = 5$ [(a7)–(d7)] cases when $\Delta\phi = \pi$ and $C_\mu = 2.149$. The spectral analysis is performed over 100 nominal natural periods of the system for the $f_{sj}^* = 0.6$ and 2.6 cases after the flow reaches its steady state, whereas for the other cases, it is conducted over 35 VIV periods.

lock-on regime or at high frequencies where it dominates the flow. However, when utilizing the primary lock-on for VIV suppression, caution must be taken in choosing a suitable SJ frequency, since as demonstrated in the present study the frequency difference between VIV suppression and VIV augmentation is small. It is also suggested to avoid operating the SJ pair in the tertiary lock-on regime because its narrow frequency range usually causes the augmentation of VIV.

Note that since the anti-phase SJ pair itself also generates small-size, anti-phase vortex pairs, the cylinder wake can never become completely symmetric and hence the vortex force can never be reduced to absolute zero, no matter how large the SJ

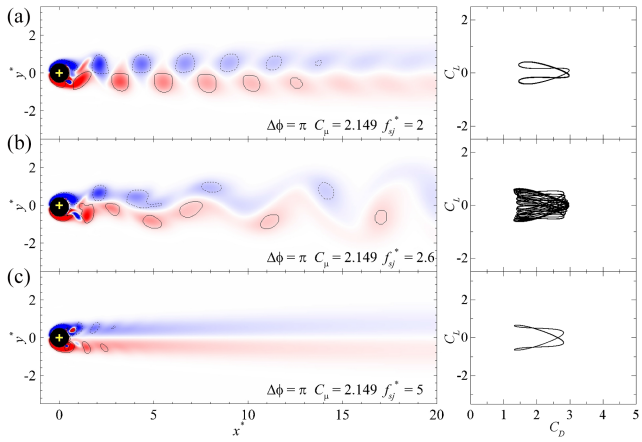

FIG. 7. Wake patterns and C_L-C_D phase diagrams for $f_{sj}^* = 2$ (a), $f_{sj}^* = 2.6$ (b), and $f_{sj}^* = 5$ (c) cases when $\Delta\phi = \pi$ and $C_\mu = 2.149$.

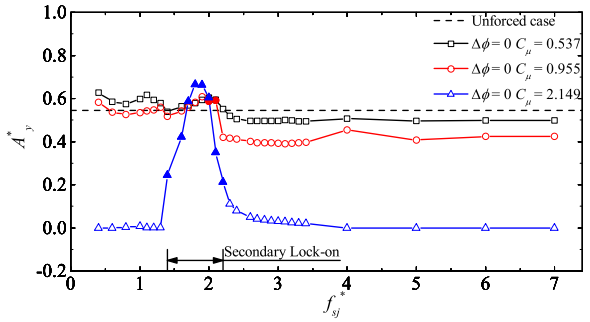

FIG. 8. The variations of the cylinder's transverse VIV amplitude (A_y^*) against the SJ frequency (f_{sj}^*) when the in-phase SJ pair is applied for VIV control. Open symbols correspond to the non-lock-on cases and solid symbols denote the lock-on cases.

strength is or what SJ frequency is used. This can be confirmed from the instantaneous wakes of the $f_{sj}^* = 2$ and 5 cases, as shown in Figs. 7(a) and 7(c). Consequently, using the anti-phase SJ pair cannot fully eliminate the cylinder's transverse VIV.

In addition to steady-state dynamics, the time histories shown in Fig. 6 also reveal the transient processes right after the SJ pair is switched on. The responsiveness of the VIV to the SJ control is well demonstrated from these transient processes, especially in the lock-on and high-frequency cases. Furthermore, the spectra shown in Fig. 6 also reveal other frequency components in addition to the two key frequencies, i.e., $f^* = 1$ and f_{sj}^*. In non-lock-on cases such as at $f_{sj}^* = 0.6$ and 2.6, these frequencies are linear combinations of the two key frequencies. As demonstrated in Figs. 6(c1) and 6(c5), only when these frequencies are close to the nominal natural frequency 1 and their corresponding C_V components are not small, their corresponding VIV components are tangible. In lock-on cases, however, since the main vortex forcing frequency is attracted to the SJ frequency or its submultiple, the linear combination of the two key frequencies is not observed. Instead, only the multiples of the SJ frequency are obtained in the C_V spectra. Since these induced multiples are far from the nominal natural frequency, no tangible VIV components are observed at their respective frequencies.

C. VIV controlled by the in-phase SJ pair

When the in-phase (i.e., $\Delta\phi = 0$) SJ pair is implemented, the cylinder's transverse VIV amplitude (A_y^*) also varies with the SJ frequency (f_{sj}^*), as shown in Fig. 8. Similar to in the anti-phase cases, the operation of SJs generally reduces the VIV amplitude, and the control becomes more effective with the increase of the SJ strength (C_μ). Therefore, the following discussion is only focused on the curve with the largest SJ strength (i.e., $C_\mu = 2.149$, in blue).

It is seen from Fig. 8 that the in-phase SJ control is very effective except in the regime near $f_{sj}^* = 2$, where a peak appears in the VIV amplitude. In this regime, the secondary lock-on occurs (denoted by solid symbols), where the vortex shedding frequency is attracted to 1/2 of the SJ frequency.[15] This is evidenced by the time histories and spectra of the cylinder's transverse displacement (y_o^*) and of the vortex force coefficient (C_V) for a representative case (forcing at $f_{sj}^* = 2$) shown in Figs. 9(a2)–9(d2), where a non-zero $f^* = 1$ component of vortex force appears, inducing the cylinder's VIV at its natural frequency.

When the SJ pair operates outside the near $f_{sj}^* = 2$ regime, unlike in the anti-phase control, complete suppression of the transverse VIV can be achieved, i.e., $A_y^* = 0$. The reason is because the in-phase operation of the SJ pair forces symmetric shedding of vortices from the cylinder that overwhelms the naturally asymmetric vortex shedding. As such, the net vortex force becomes absolute zero and no transverse VIV occurs after the flow reaches its steady state. This successful VIV suppression is well demonstrated in two representative cases, i.e., the $f_{sj}^* = 1.2$ case that is far less than the lock-on frequency and the $f_{sj}^* = 5$ case that is far greater, as shown in Fig. 9. The forced symmetric wakes and C_L-C_D phase diagrams for these two cases are also shown in Fig. 10. The horizontal lines obtained in the phase diagrams indicate that while the transverse VIV has been successfully suppressed, the drag experienced by the cylinder still fluctuates wildly. However, although not captured in the present frequency range, it is believed that the VIV will revive when f_{sj}^* becomes much smaller than the natural frequency. This is because the interruption of the vortex evolution process and hence the VIV control is mainly realized by the blowing stroke of the SJ.[15] As f_{sj}^* decreases, the natural vortex shedding will gradually recover during the suction stroke and so does the VIV.

D. VIV controlled by the SJ pair with intermediate phase differences

When the SJ pair operates at $C_\mu = 2.149$ with the other intermediate phase differences, i.e., $\Delta\phi = \pi/4$, $\pi/2$, and $3\pi/4$, different from the in-phase and anti-phase cases, all the primary, secondary, and tertiary lock-on can be induced, as indicated by the three major peaks shown in Fig. 11. It is found that the lock-on range and VIV amplitude (A_y^*) in the secondary lock-on regime decrease with the increase of phase difference, whereas in the tertiary lock-on regime, the trend is reversed. This trend does not apply in the primary lock-on regime though. On its right branch (i.e., $f_{sj}^* \geq 1$), the lock-on range extends with the increase of phase difference as expected. On its left branch (i.e., $f_{sj}^* < 1$), however, this range

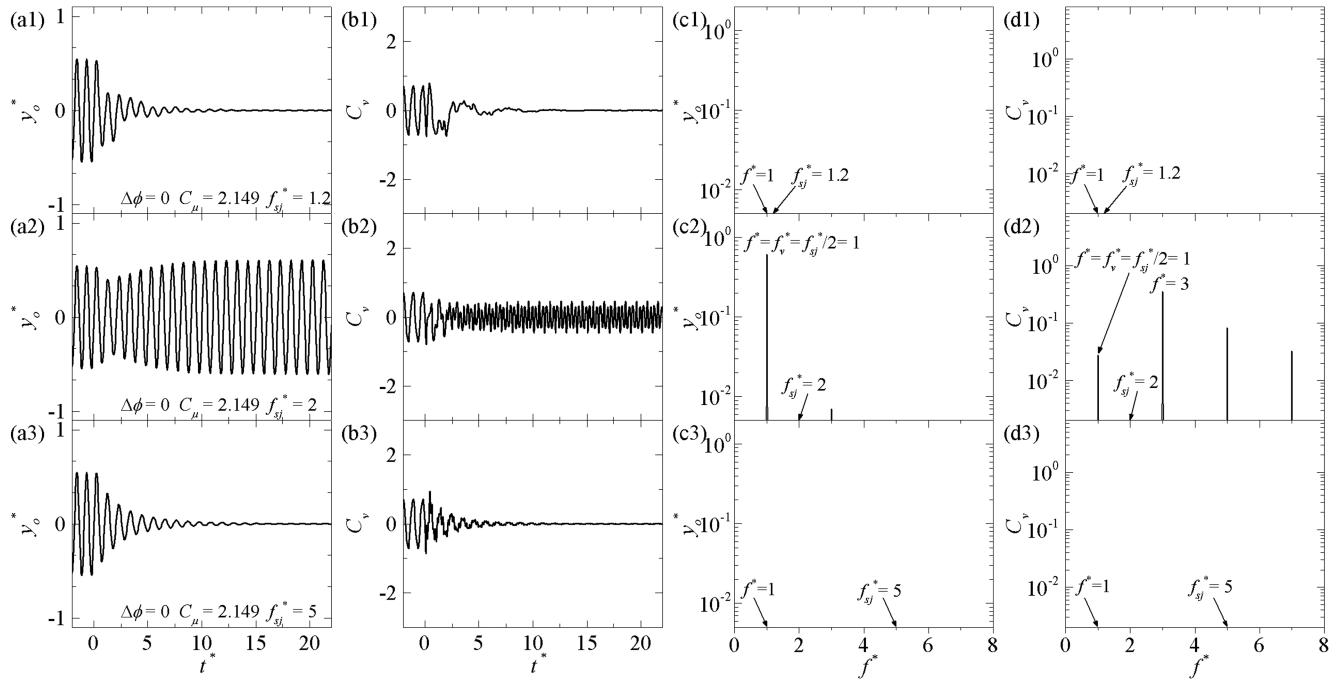

FIG. 9. Time histories and frequency spectra of the normalized cylinder's y-displacement (y_o^*) and the cross-flow vortex force coefficient (C_V) for $f_{sj}^* = 1.2$ [(a1)–(d1)], $f_{sj}^* = 2$ [(a2)–(d2)], and $f_{sj}^* = 5$ [(a3)–(d3)] cases when $\Delta\phi = 0$ and $C_\mu = 2.149$. The spectral analysis is performed over 35 VIV periods after the flow reaches its steady state.

variation is not seen. At $f_{sj}^* \geq 4$, all the curves level off and become indistinguishable, confirming that the SJ pair is effective in suppressing the VIV regardless of the operating phase difference.

Furthermore, in the range of $f_{sj}^* < 1$, obvious A_y^* fluctuations are observed in the curves with intermediate phase differences. It is found that at $f_{sj}^* = 0.4$, the VIV amplitudes become even larger than that in the unforced case. This is a consequence of the occurrence of a new kind of lock-on phenomenon, termed as superharmonic lock-on, in which the vortex shedding frequency is attracted to a multiple of the SJ frequency.[15] This superharmonic lock-on is evidenced in the time histories and frequency spectra of a representative case with $\Delta\phi = 3\pi/4$ and $f_{sj}^* = 0.4$, as plotted in Fig. 12. In this case, the vortex shedding frequency is shifted to $f^* = 2f_{sj}^* = 0.8$, and high spectral peaks in C_V and y_o^* can be observed at both f_{sj}^* and $2f_{sj}^*$. Since $f^* = 0.8$ is still close to the cylinder's natural frequency, the C_V and y_o^* oscillations are intensified by the operation of the SJ pair. This, again, confirms that the VIV could also be augmented by the occurrence of lock-on.

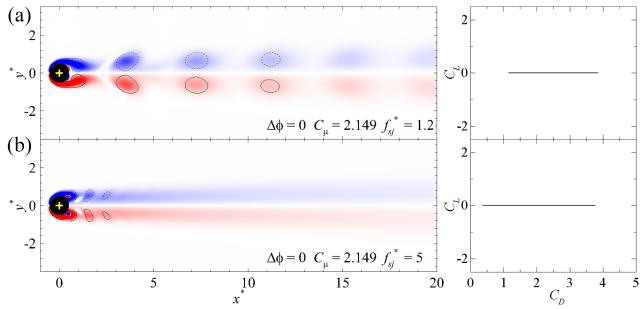

FIG. 10. Wake patterns and C_L-C_D phase diagrams for $f_{sj}^* = 1.2$ (a) and $f_{sj}^* = 5$ (b) cases when $\Delta\phi = 0$ and $C_\mu = 2.149$.

E. Influence of the SJ pair on drag

In addition to the influence on lift, the application of the SJ pair also affects the drag experienced by the cylinder. Figure 13 shows the variations of time-averaged drag coefficient ($\bar{C}_D$) against the SJ frequency when the anti-phase or in-phase SJ pair is applied with the largest momentum coefficient $C_\mu = 2.149$. It is seen that in the vicinity of the primary and tertiary lock-on as well as in the regime between these two lock-on, the operation of the anti-phase SJ causes the increase of mean drag if compared with the value of the unforced case ($\bar{C}_D = 2.162$, represented by the horizontal dashed line). The same trend is also observed in the vicinity of the secondary

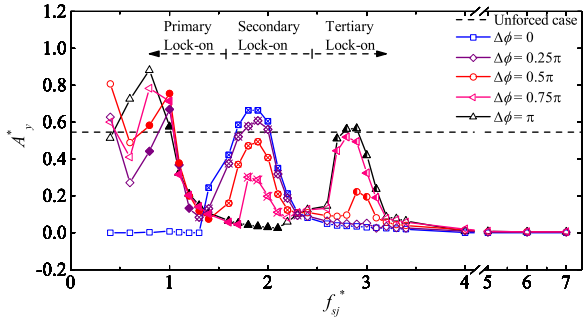

FIG. 11. The variations of the cylinder's transverse VIV amplitude (A_y^*) against the SJ frequency (f_{sj}^*) when the SJ momentum coefficient $C_\mu = 2.149$ and phase difference $\Delta\phi = 0$, $\pi/4$, $\pi/2$, $3\pi/4$, and π. Solid symbols denote the primary lock-on cases, crossed symbols represent the secondary lock-on cases, half-solid symbols correspond to the tertiary lock-on, and open symbols indicate the non-lock-on or other lock-on cases.

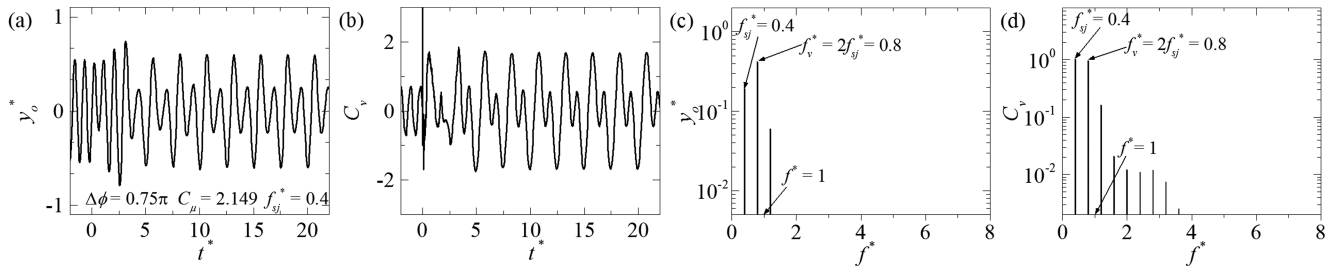

FIG. 12. Time histories and frequency spectra of the normalized cylinder's y-displacement (y_o^*) and the cross-flow vortex force coefficient (C_V) for $f_{sj}^* = 0.4$ case when $\Delta\phi = 3\pi/4$ and $C_\mu = 2.149$. The spectral analysis is performed over 35 VIV periods after the flow reaches its steady state.

lock-on when the in-phase SJ is applied. This indicates that the occurrence of lock-on causes the increase of drag, no matter whether it suppresses or augments the lift fluctuation and the resulting transverse VIV. In both SJ settings, the mean drag gradually levels off to a lower value of 2.06 when the SJ pair operates at frequencies higher than 3.5. The slight reduction of the mean drag at high frequencies is mainly due to the non-zero momentum injection by the SJ pair. Therefore, if taking the resulting drag into consideration, one can say that the best VIV control is realized at higher SJ frequencies.

F. DMD analysis

The dynamic mode decomposition (DMD) method is a useful tool for extracting coherent flow structures from unsteady flows. Different from another popular method, i.e., the proper orthogonal decomposition (POD) method that extracts flow structures based on their fluctuating energy ranking,[27] DMD extracts flow structures based on their contributions to flow dynamics. Or in another word, it is able to extract spatial modes based on their frequency content. This great feature makes DMD an effective spectral method for analyzing dynamics of a flow system involving multiple frequency components like in this study.[28]

Through the DMD method, a series of DMD modes at their corresponding frequencies can be obtained, and the flow velocity field ($\boldsymbol{v}$) can be re-constructed using the first L DMD modes as[29]

$$\boldsymbol{v}(\boldsymbol{x}, t) = \sum_{i=0}^{L \le N} a_i e^{\lambda_i t} \boldsymbol{\Phi}_i(\boldsymbol{x}), \tag{18}$$

where N is the total number of snapshots, and a_i and λ_i are the amplitude and frequency of the ith DMD mode ($\boldsymbol{\Phi}_i$), respectively. More details about the DMD method and its algorithm can be found in the studies of Schmid[28] and Sayadi *et al.*[29]

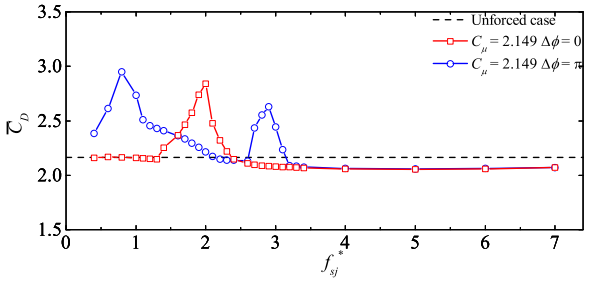

FIG. 13. The variations of cylinder's time-averaged drag coefficient ($\bar{C}_D$) against the SJ excitation frequency (f_{sj}^*) when $C_\mu = 2.149$ and $\Delta\phi = 0$ and π.

In the present study, DMD analyses are conducted to reveal more flow physics related to the SJ-based VIV suppression. 6 representative cases are selected, including one unforced, three anti-phase controlled (SJ frequency $f_{sj}^* = 1.2$, 2.8, and 5 with SJ momentum coefficient $C_\mu = 2.149$), and two in-phase controlled cases ($f_{sj}^* = 1.2$ and 2.1 with $C_\mu = 2.149$). Note that only the cases that show periodic wakes are selected for the analysis so that effective comparison of DMD modes can be made. In all these cases, DMD analyses are performed in a subdomain of the original computational domain, ranging from $x^* = 0.53$ to 8 and from $y^* = -2.5$ to 2.5 that covers the downstream flow field of the oscillating cylinder. Also, due to the periodicity of the flow, the analyses are conducted over just one VIV period, within which more than 100 equi-interval snapshots of the flow field are selected. Although not presented here for brevity, it has been confirmed that this number of snapshots is sufficiently large to produce convergent results in all selected cases.

Figure 14 shows the distribution of the DMD mode amplitude ($|a_i|$) in the first row, the original wakes in the second row, the first three DMD modes of the decomposed wakes in the third to fifth rows, and the wakes superimposing the first three modes in the last row, for the six selected cases. In the unforced case, the $|a_i|$ distribution shown in Fig. 14(a) reveals that mode 0 at $f^* = 0$, mode 1 at $f^* = 1.1$, and mode 2 at $f^* = 2.2$ are three dominant modes in this dynamic flow system. Higher-order modes also contribute to the dynamics, indicating the nonlinearity of the system. Mode 0 shown in Fig. 14(a2) represents the time-averaged flow field, where a pair of shear layers appears symmetrically about the channel centerline. In mode 1 [Fig. 14(a3)], two counter-rotating vortices are produced in sequence within one VIV period, each first appearing behind the cylinder along the channel centerline and then gradually evolving into two smaller co-rotating vortices downstream. Since any of the two counter-rotating vortices can affect the circulation around the cylinder, such vortices cause the fluctuation of lift force. Therefore, it is mode 1 that mainly contributes to the fluctuation of lift force and hence the cylinder's transverse oscillation. Similarly, the fluctuation of drag force is mainly caused by mode 2, where two pairs of counter-rotating vortices are generated within half a VIV period, with their sign of vorticity swapped. If superimposing these three modes together, the vorticity contours with the same sign are strengthened, while those with opposite signs are

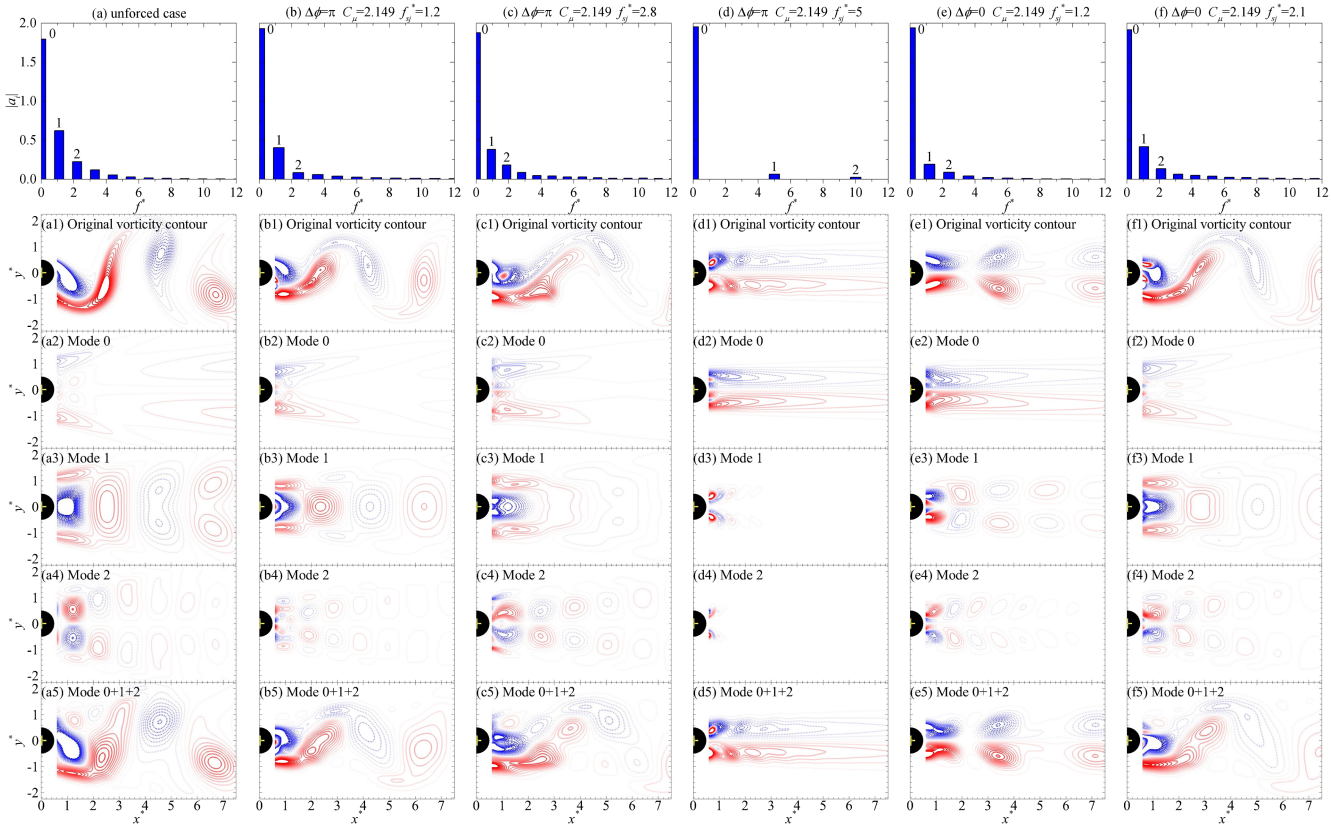

FIG. 14. Mode amplitude ($|a_i|$) versus normalized frequency (f^*) as well as the vorticity contours of the original wake [(a1)–(f1)], mode 0 [(a2)–(f2)], mode 1 [(a3)–(f3)], mode 2 [(a4)–(f4)], and mode 0+1+2 [(a5)–(f5)] for the unforced case (a) and the cases of $f_{sj}^* = 1.2$ (b), 2.8 (c), and 5 (d) when $\Delta\phi = \pi$ and $C_\mu = 2.149$ as well as the cases of $f_{sj}^* = 1.2$ (e) and 2.1 (f) when $\Delta\phi = 0$ and $C_\mu = 2.149$.

attenuated. Through this superimposition, the major features of the original Kármán vortex street can be recovered in the re-constructed field (mode 0+1+2), if comparing Figs. 14(a1) and 14(a5).

The introduction of the SJ pair, either anti-phase or in-phase, certainly affects the dominant DMD modes. As the SJ pair induces lock-on, i.e., the primary lock-on at $f_{sj}^* = 1.2$ [Fig. 14(b)], the secondary lock-on at $f_{sj}^* = 2.1$ [Fig. 14(f)], and the tertiary lock-on at $f_{sj}^* = 2.8$ [Fig. 14(c)], the frequencies of mode 1 and mode 2 shift accordingly, as revealed in their respective spectra. Other than this change, although slight difference can be observed, these dominant modes still look similar to those in the unforced case, mainly because of the occurrence of lock-on.

As the anti-phase SJ pair operates at higher frequencies, such as at $f_{sj}^* = 5$ [Fig. 14(d)], the two shear layers appearing in mode 0 [Fig. 14(d2)] are much closer to the centerline, indicating a small transverse VIV amplitude in this case. In addition, mode 1 located at $f^* = 5$ is dominated only by the SJ flow appearing in the near field, which is quite different from the unforced and three lock-on cases. The lack of a mode around $f^* = 1$ again confirms that the natural vortex shedding is completely suppressed. However, the anti-phase SJ pair produces co-rotating vortices as shown in mode 1 so that the superimposed flow field can never be symmetric about the centerline, especially in the near field. As such, the lift experienced by the cylinder can never be settled at absolute zero.

As the in-phase SJ pair operates at frequencies outside the secondary lock-on regime, such as at $f_{sj}^* = 1.2$ [Fig. 14(e)], a very small transverse VIV amplitude is also achieved, which is implied by the two near-centerline shear layers shown in mode 0. In this case, mode 1 is also shifted to the SJ frequency. But this does not mean the occurrence of lock-on because in mode 1 the typical sequence of counter-rotating vortices along the centerline does not appear as in the unforced and three lock-on cases. Instead, new flow structures—a sequence of vortex pairs with alternative signs—appear in mode 1, due to the strong symmetry imposed by the SJ pair. As a result, the superimposed flow field can be absolutely symmetric and hence the lift experienced by the cylinder can be settled at absolute zero.

IV. CONCLUSION

This paper studies the active VIV control of a circular cylinder using a SJ pair at a low Reynolds number of 100. The SJ pair operates with various phase differences over a wide frequency range so that the effects of various lock-on on the VIV control can be investigated. The major findings are as follows:

1. The VIV control can be affected not only by the occurrence of primary lock-on as reported by Du and Sun[11] but also by the occurrence of other lock-on such as secondary, tertiary, and even superharmonic lock-on as revealed in the present study.

2. While the occurrence of lock-on can shift the frequency of vortex shedding, it does not always result in successful VIV suppression. Sometimes it even causes the augmentation of VIV. First, the frequency difference between VIV suppression and augmentation is small, as demonstrated in the vicinity of the primary lock-on in the present study. Second, the occurrence of a higher or lower order lock-on is usually within a narrow operational frequency range, causing the augmentation of VIV as demonstrated in the secondary, tertiary, and superharmonic lock-on regimes in the present study.
3. When the SJ pair operates with the intermediate phase differences, i.e., $\Delta\phi = \pi/4$, $\pi/2$, and $3\pi/4$, the superharmonic, primary, secondary, and tertiary lock-on can all be induced. Its capability in the VIV control in lock-on regimes generally lies in between those of the in-phase and anti-phase cases.
4. Compared to the control by means of lock-on, the VIV suppression using general in-phase operation or high-frequency operation of the SJ pair, i.e., the conventional vortex-strength-reduction method, seems more effective. Furthermore, by taking the influence on drag into account, the best VIV control using the SJ pair is realized at high SJ frequencies.
5. The DMD analyses reveal that the dominant modes in lock-on cases are similar to those in the unforced case. In successful non-lock-on control cases, the difference is significant, especially in mode 1 where the flow structures determining the asymmetry of wake are captured.

This work furthers our understanding in the influence of active lock-on on the VIV control. The results reported are still limited because the lock-on is induced only at a low Reynolds number 100. At higher Reynolds numbers, the spanwise instability will result in an intrinsic three-dimensional flow, making the analysis and control more challenging. In the near future, the VIV control by the SJ pair at higher Reynolds numbers will be systematically investigated.

ACKNOWLEDGMENTS

The authors gratefully acknowledge the financial support for this study from the Research Grants Council of Hong Kong under General Research Fund (Project No. PolyU 152493/16E).

[1]H. Choi, W. P. Jeon, and J. S. Kim, "Control of flow over a bluff body," Annu. Rev. Fluid Mech. **40**, 113–139 (2008).
[2]M. M. Zdravkovich, "Review and classification of various aerodynamic and hydrodynamic means for suppressing vortex shedding," J. Wind Eng. Ind. Aerodyn. **7**, 145–189 (1981).
[3]H. Oertel, Jr., "Wakes behind blunt bodies," Annu. Rev. Fluid Mech. **22**, 539–562 (1990).
[4]O. M. Griffin and M. S. Hall, "Review-vortex shedding lock-on and flow control in bluff body wakes," J. Fluids Eng. **113**, 526–537 (1991).
[5]I. Korkischko and J. R. Meneghini, "Suppression of vortex-induced vibration using moving surface boundary-layer control," J. Fluids Struct. **34**, 259–270 (2012).
[6]S. Dong, G. S. Triantafyllou, and G. E. Karniadakis, "Elimination of vortex streets in bluff-body flows," Phys. Rev. Lett. **100**, 204501 (2008).
[7]C. Wang, H. Tang, S. Yu, and F. Duan, "Active control of vortex-induced vibrations of a circular cylinder using windward-suction-leeward-blowing actuation," Phys. Fluids **28**, 053601 (2016).
[8]C. Wang, H. Tang, F. Duan, and S. Yu, "Control of wakes and vortex-induced vibrations of a single circular cylinder using synthetic jets," J. Fluids Struct. **60**, 160–179 (2016).
[9]W. L. Chen, H. Li, and H. Hu, "An experimental study on a suction flow control method to reduce the unsteadiness of the wind loads acting on a circular cylinder," Exp. Fluids **55**, 1–20 (2014).
[10]K. B. Skaugset and C. M. Larsen, "Direct numerical simulation and experimental investigation on suppression of vortex induced vibrations of circular cylinders by radial water jets," Flow, Turbul. Combust. **71**, 35–59 (2003).
[11]L. Du and X. Sun, "Suppression of vortex-induced vibration using the rotary oscillation of a cylinder," Phys. Fluids **27**, 023603 (2015).
[12]S. J. Baek and H. J. Sung, "Quasi-periodicity in the wake of a rotationally oscillating cylinder," J. Fluid Mech. **408**, 275–300 (2000).
[13]S. J. Baek, S. B. Lee, and H. J. Sung, "Response of a circular cylinder wake to superharmonic excitation," J. Fluid Mech. **442**, 67–88 (2001).
[14]J. S. Leontini, D. L. Jacono, and M. C. Thompson, "Wake states and frequency selection of a streamwise oscillating cylinder," J. Fluid Mech. **730**, 162–192 (2013).
[15]C. Wang, H. Tang, S. Yu, and F. Duan, "Lock-on of vortex shedding to a pair of synthetic jets with phase difference" (unpublished).
[16]L. Du, X. Jing, and X. Sun, "Modes of vortex formation and transition to three-dimensionality in the wake of a freely vibrating cylinder," J. Fluids Struct. **49**, 554–573 (2014).
[17]R. Govardhan and C. Williamson, "Modes of vortex formation and frequency response of a freely vibrating cylinder," J. Fluid Mech. **420**, 85–130 (2000).
[18]S. S. Rao and F. F. Yap, *Mechanical Vibrations*, 5th ed. (Prentice Hall, 2011), Vol. 4.
[19]R. Bourguet and D. Lo Jacono, "In-line flow-induced vibrations of a rotating cylinder," J. Fluid Mech. **781**, 127–165 (2015).
[20]P. Lallemand and L. Luo, "Theory of the lattice Boltzmann method: Dispersion, dissipation, isotropy, galilean invariance, and stability," Phys. Rev. E **61**, 6546–6562 (2000).
[21]D. Yu, R. Mei, and W. Shyy, "A multi-block lattice Boltzmann method for viscous fluid flows," Int. J. Numer. Methods Fluids **39**, 99–120 (2002).
[22]P. Lallemand and L. S. Luo, "Lattice Boltzmann method for moving boundaries," J. Comput. Phys. **184**, 406–421 (2003).
[23]Y. Chen, Q. Cai, Z. Xia, M. Wang, and S. Chen, "Momentum-exchange method in lattice Boltzmann simulations of particle-fluid interactions," Phys. Rev. E **88**, 013303 (2013).
[24]S. Izquierdo and N. Fueyo, "Characteristic nonreflecting boundary conditions for open boundaries in lattice Boltzmann methods," Phys. Rev. E **78**, 046707 (2008).
[25]J. Zhou, R. J. Adrian, S. Balachandar, and T. M. Kendall, "Mechanisms for generating coherent packets of hairpin vortices in channel flow," J. Fluid Mech. **387**, 353–396 (1999).
[26]C. H. K. Williamson and A. Roshko, "Vortex formation in the wake of an oscillating cylinder," J. Fluids Struct. **2**, 355–381 (1988).
[27]C. W. Rowley, I. Mezić, S. Bagheri, P. Schlatter, and D. S. Henningson, "Spectral analysis of nonlinear flows," J. Fluid Mech. **641**, 115–127 (2009).
[28]P. J. Schmid, "Dynamic mode decomposition of numerical and experimental data," J. Fluid Mech. **656**, 5–28 (2010).
[29]T. Sayadi, P. Schmid, J. W. Nichols, and P. Moin, "Dynamic mode decomposition of controlled h-and k-type transitions," Annu. Res. Briefs **2013**, 189–200, available at https://web.stanford.edu/group/ctr/ResBriefs/2013/14_sayadi.pdf.